Iron ore tailings as fine mineral aggregate in asphalt mixtures

Rejeito de minério de ferro como agregado mineral fino em misturas asfálticas

Igor Castro Sá de Oliveira[1], Adalberto Leandro Faxina[2]

[1]University of São Paulo, São Paulo – Brazil, oliveira.igor@usp.br
[2]University of São Paulo, São Paulo – Brazil, adalberto@usp.br

ABSTRACT
The growing mineral production generates gradually higher volumes of solid waste, motivating studies to be carried out to enable the use of this waste in several fields. The main objective of this paper is to evaluate the use of iron ore tailings (IOT) from flotation process (which resembles fine sand) in the composition of asphalt mixtures. Asphalt mixtures and fine aggregate matrices (FAMs) were produced with gneiss aggregates and IOT. The asphalt mixtures were evaluated by means of tensile strength test and moisture-induced damage test. The FAMs were subjected to fatigue tests in the dynamic shear rheometer, and fatigue models were built for non-conditioned and moisture-conditioned specimens. The greater adhesiveness of the asphalt binder to the IOT provided greater tensile strength to the asphalt mixtures and increased the fatigue life of the moisture-conditioned FAM specimens. The overall conclusion is that the asphalt mixtures and the FAMs prepared with IOT showed lower moisture susceptibility.

RESUMO
A crescente produção mineral gera volumes gradativamente maiores de resíduos sólidos, motivando a realização de estudos que viabilizem o aproveitamento desses resíduos em outras áreas. O objetivo deste trabalho é avaliar a utilização do rejeito de flotação do minério de ferro, que se assemelha a uma areia fina, como material constituinte de misturas asfálticas. Foram produzidas misturas asfálticas completas (MAC) e matrizes de agregados finos (MAF) empregando agregados de gnaisse e rejeito de minério de ferro. A MAC foi avaliada por meio da resistência à tração e dano por umidade induzida. As MAFs foram submetidas a ensaios de fadiga no reômetro de cisalhamento dinâmico, gerando modelos de fadiga das amostras com e sem condicionamento à umidade. A melhor adesividade do ligante asfáltico ao rejeito proporcionou maior resistência à tração na MAC e maior vida de fadiga à MAF condicionada, além de reduzir a suscetibilidade à umidade nas duas escalas.

1. INTRODUCTION

The mineral production showed a significant growth in the last years, particularly in Brazil. The production value of the 11 main metallic minerals increased from U$ 24.0 billion in 2009 to U$ 48.6 billion in 2019, representing a growth of 102.5 % (ANM, 2020). These data indicate a strong trend of growth of the mining activities in the coming years, which highlights its enormous economic and social relevance. On the other hand, the volume of waste materials derived from this economic activity is increasing, and the areas for its appropriate disposal in the environment are scarce. Moreover, in case of ineffective mechanisms for the correct disposal and monitoring of these materials, several regions and populations will be at risk of being

negatively affected by accidents of catastrophic consequences. This is the most relevant environmental impact of mining, especially in the case of iron ore, which represents the largest volume of all processed minerals in Brazil. For these reasons, it is essential to develop studies that make the use of the residues derived from mineral exploration possible. The use of iron ore tailing (IOT) as construction material can be a solution to add value to this byproduct. In addition to this, it can minimize the environmental impacts of mineral exploration.

The IOT obtained by the flotation process of iron ore presents characteristics that allow its use as raw material for the production of asphalt concrete or Portland cement concrete. The evaluation of these tailings from different regions revealed that the particle size distribution (PSD) of this material resembles fine and medium sands, with predominance of irregular particles (Fernandes, 2005; Campanha, 2011; Silva *et al.*, 2015; Galhardo, 2015; Bastos *et al.*, 2016; Sant'ana Filho *et al.*, 2017; Souza *et al.* 2020). As for environmental classification as per Brazilian regulations, the tailings were classified as Class II A, non-hazardous and non-inert solid waste (Fernandes, 2005; Silva *et al.*, 2015; Galhardo, 2015; Bastos *et al.*, 2016), and Class II B, non-hazardous and inert (Sant'ana Filho *et al.*, 2017; Souza *et al.* 2020).

Recent studies pointed out that the use of tailings in pavement layers can be technically and economically feasible. Campanha (2011), Galhardo (2015), and Bastos *et al.* (2016) approached the use of the IOT as soil stabilizing material and the IOT itself stabilized with hydraulic binders. The aforementioned researchers carried out laboratory tests, such as compressive strength, resilient modulus, durability and expansion, and concluded that the use of the tailings in base and subbase layers may be technically and economically feasible, provided that they are stabilized with Portland cement or hydrated lime in appropriate proportions. Kumar *et al.* (2014), Silva *et al.* (2015), and Sant'ana Filho *et al.* (2017) used IOT to replace the fine sand in the production of interlocked concrete blocks, and concluded that the blocks produced with IOT met the minimum compressive strength needed to withstand regular vehicle traffic. In addition, no variation in the block dimensions were observed when they were submitted to water immersion cycles.

Silva and Fernandes (2013), Wang *et al.* (2016), Apaza *et al.* (2018), and Souza *et al.* (2020) assessed the mechanical behavior of asphalt mixtures compounded with IOT in substitution for fine aggregates and fillers, by means of the following tests: exudation, resilient modulus, and tensile strength and fatigue by diametrical compression. Such mixtures showed mechanical behavior comparable to the conventional ones, which led those researchers to conclude that the use of IOT in asphalt mixtures may be technically feasible. However, Souza *et al.* (2020) noticed that the mixtures prepared with tailings resulted more susceptible to permanent deformations. They warned that a careful evaluation of the climatic conditions and traffic volume should be done to avoid rutting.

When it comes to the characterization of damage in asphalt mixtures, many researchers chose to carry out tests with the fine aggregate matrix (FAM) of the asphalt mixtures. FAM is defined as a composite comprised of fine aggregates and mastic, which represents the internal structure of the asphalt concrete. As claimed by several researchers, fatigue cracking and moisture damage are phenomena typically related to the fine portion of the asphalt mixtures (Kim, Little e Song, 2003; Zollinger, 2005; Bhasin, 2006; Masad *et al.*, 2006; Arambula, Masad e Martin, 2007; Caro *et al.*, 2008a, 2008b; Castelo Branco *et al.*, 2008; Vasconcelos, Little e Bhasin, 2010; Coutinho *et al.* 2010; Vasconcelos et al, 2011; Coutinho, 2012; Sousa *et al.*, 2013; Underwood e Kim, 2013; Karki, Li e Bhasin, 2015; Gudipudi e Underwood, 2015, 2017; Freire *et al.*, 2017; Fonseca *et al.*, 2019; Rodrigues *et al.* 2019). One of the approaches adopted in studies on fatigue

characterization is based on the viscoelastic continuum damage theory (VECD). The 50% reduction in pseudostiffness, C, has been adopted as a criterion for fatigue failure, and the microstructural changes within the material are quantified by the internal state variable, S, which represents the damage state of the material (Castelo Branco *et al.* 2008; Palvadi, 2011; Coutinho, 2012; Palvadi, Bhasin e Little, 2012; Gudipudi e Underwood, 2017; Ng, 2017; Klug, 2017).

The main objective of this study was to add the IOT derived from the flotation process in substitution for the fine gneiss aggregates in asphalt mixtures and fine aggregate matrices (FAMs). The materials used here have the same origin as those applied in a trial section built at the Cauê mine (VALE S.A.) in the city of Itabira/MG, Brazil. The asphalt mixtures were evaluated by means of the tensile strength and moisture-induced damage tests. The reference and moisture-conditioned FAMs were evaluated by means of fatigue tests carried out on the dynamic shear rheometer (DSR).

2. MATERIALS AND METHODS
2.1. Iron ore tailings from the flotation process

The iron ore tailings used in this study came from the iron ore flotation process, which was collected before being laid in a dam. This residue was classified as class II A solid residue - non-hazardous and non-inert. Oliveira (2017) and Campos and Santos (2017) carried out IOT characterization tests, the results of which are as follows: (i) density (DNER-ME 084/95 method): 2.985 g/cm³; (ii) sand equivalent (DNER-ME 054/97 method): 59.24%; and (iii) X-ray diffraction, to obtain the mineralogical composition of the IOT: Fe_2O_3 (3.8%) and SiO_2 (96.2%). In addition, the IOT's PSD was determined by means of the sedimentation test (NBR 7181/2016). The IOT´s PSD is presented in Figure 1, together with the PSD of the gneiss fine aggregate (stone powder). The IOT had particle sizes smaller than 0.42 mm in diameter, resembling the PSD of a fine sand according to the ABNT NM 248/2001 specification.
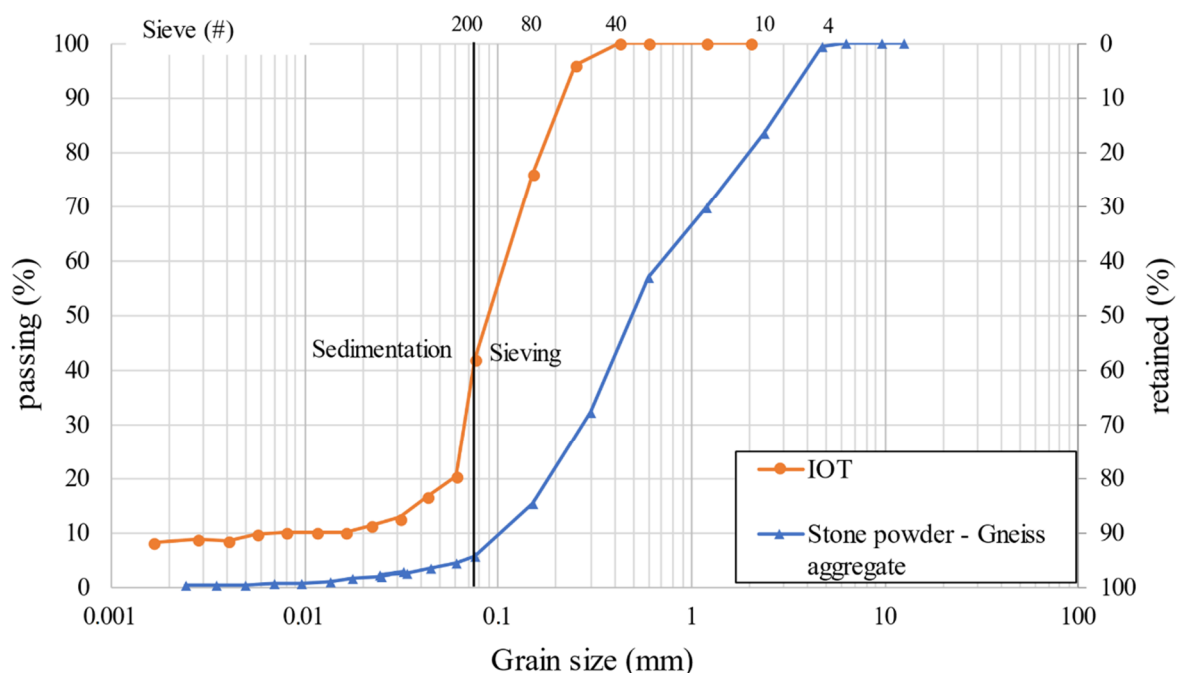
Figure 1. Particle size distribution (sieving + sedimentation) of the fine fractions

2.2. Gneiss aggregates

The mineral aggregates used in this study are derived from rocky matrices of gneiss, which were supplied by Belmont quarry (Itabira/MG). Table 1 presents some characteristics of the mineral aggregate and the respective test methods prescribed by the Brazilian Department of Transportation Infrastructure (DNIT). The aggregate meets the specification for the shape factor, but it did not meet the particle shape criterion (percentage of lamellar particles). Such a drawback may compromise the asphalt mixture performance, as lamellar particles tend to break during compaction, increasing the contact surface between aggregate and asphalt binder, in addition to increasing the voids of the mineral aggregate (Prowell *et al.*, 2005).

Table 1 – Characteristics of the mineral aggregates

Characteristic	Material	Method	Result	Allowable values
Los Angeles abrasion (%)	Coarse aggregate	NBR NM 51	43.70	< 50
Mechanical strength (10% of fines) (%)	Coarse aggregate	DNER-ME 096/98	8.51	< 10
Particle shape (% lamellar)	Coarse aggregate	NBR 5564	15.50	< 10
Shape factor	Coarse aggregate	NBR 5564	2.27	> 0,5
Soundness (% average loss)	Coarse aggregate	DNER-ME 089/94	1.56	< 12
Density (g/cm³)	Coarse aggregate	DNER-ME 195/97	2.748	-
	Fine aggregate		2.698	-
	Filler	DNER-ME 194/98	2.703	-
Absorption (%)	Coarse aggregate	DNER-ME 195/97	0.41	-
	Fine aggregate		1.44	-
Sand Equivalent (%)	Filler	DNER-ME 194/98	78.03	> 55

2.3. Asphalt Binder

The asphalt binder used in this study is a 50/70 pen-grade binder, which is graded as PG 64-16 according to the Superpave specification (ASTM D6373-16). Table 2 presents the results of the characterization tests of this binder.

2.4. Asphalt Mixtures: design and compaction
2.4.1. Hot Mix Asphalt (HMA) mixes

Two asphalt mixtures were designed according to ASTM D 6926-13. One of the mixtures was produced with gneiss mineral aggregates, and it is referred to as control (HMA 01). The other one was produced with IOT to replace the fractions retained in the sieves #80, #200 and bottom, and it is referred to as HMA 02. The aggregate gradation of the mixtures matches the center of the *C* band of the standard DNIT 031-ES (2006), the same defined for the trial section built at Cauê mine (Itabira/MG). The design binder content was obtained for a target air voids of 4.0%, resulting in 5.4% for HMA 01 and 5.6% for HMA 02. This slight increase in the asphalt content is due to the finer particle sizes of the IOT as compared to the fine gneiss aggregates. The HMA design information was used to perform the Fine Aggregate Matrices (FAM) design, as presented in the next item.

2.4.2. Fine Aggregate Matrices (FAMs)

Sousa *et al.* (2013) devised an experimental method to determine the FAM asphalt content, by assuming that the proportion of fine aggregates in both the FAM and asphalt mixture is the same, after normalizing it according to the FAM aggregate maximum nominal diameter. The cutting sieve used in this study was sieve #10 (2.00 mm). Figure 2 presents the PSD curves for the HMA mix and FAM.

Table 2 – Results of the binder characterization tests

Characteristic	Method (ASTM)	Result	Allowable values
Density at 25 °C [g/cm³]	D 70	1.011	-
Penetration (100 g/25 °C/5 s) [0.1 mm]	D 5	50	50 to 70
Softening point [°C]	D 36	50	> 46
Flash point [°C]	D 92	382	> 235
Ductility at 25 °C [cm]	D 113	> 150	> 60
Trichloroethylene Solubility [%]	D 2042	99.9	> 99.5
Brookfield Viscosity (135 °C/20 rpm) [cP]	D 4402	312	> 274
Brookfield Viscosity (150 °C/40 rpm) [cP]	D 4402	160	> 112
Brookfield Viscosity (177 °C/100 rpm) [cP]	D 4402	61	57 to 285
Mixing temperature [°C]	-	146-152	°C
Compaction temperature [°C]	-	135-140	°C
Dynamic shear (G*/sin δ) [kPa]	D 7175	1.19 (64 °C) 0.55 (70 °C)	> 1.00
After RTFOT (ASTM D 2872)			
Mass variation [%]	D 2872	-0.22	< 0.5
Ductility at 25 °C [cm]	D 113	> 150	> 20
Softening point increase [°C]	D 36	4.6	< 8
Retained penetration [%]	D 5	64	> 55
Dynamic shear (G*/sin δ) [kPa]	D 7175	2.39 (64 °C) 1.06 (70 °C)	> 2.20
After PAV (ASTM D 6521)			
S – stiffness modulus [MPa]	D 6648	142.5 (-06 °C) 345.9 (-12 °C)	< 300
m – relaxation rate	D 6648	0.35 (-06 °C) 0.29 (-12 °C)	> 0.3
Critical temperature – 10 °C [°C]	D 6648	-21	-
PG classification	64-16		
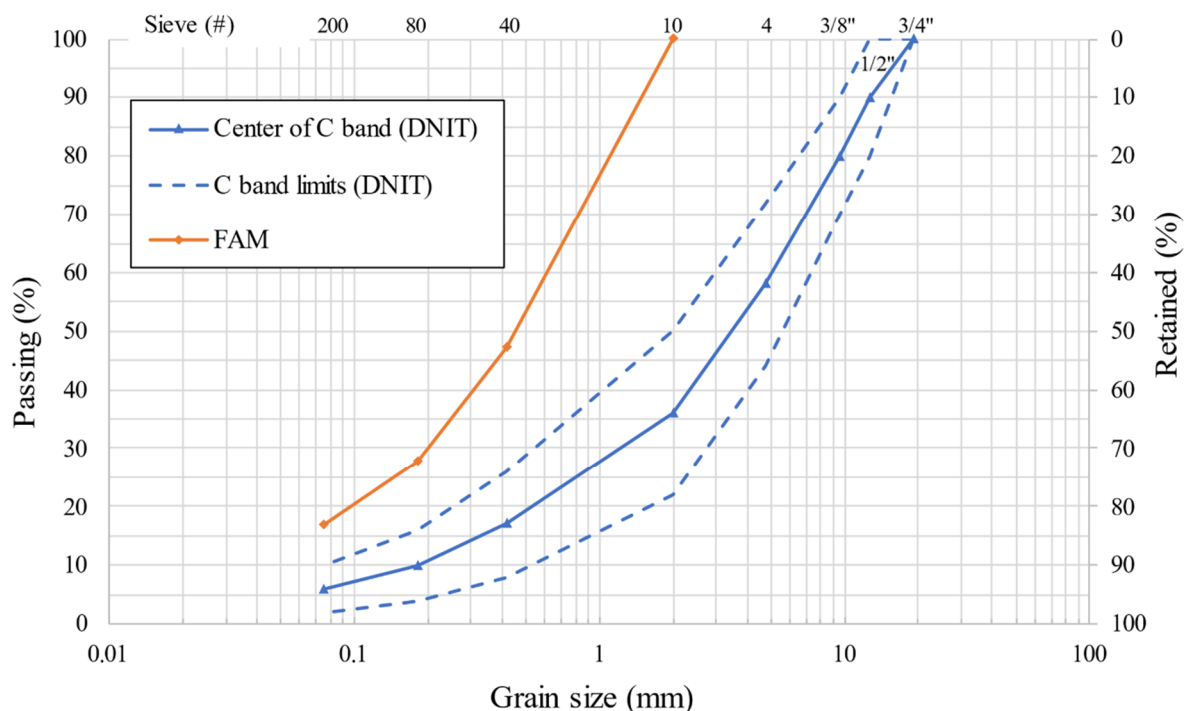
Figure 2. Particle size distribution of the HMA mix and FAM

The method proposed by Sousa *et al.* (2013) comprises the following steps: (i) prepare three loose portions of each asphalt mixture with the design binder content determined as per AASTHO T 209; (ii) condition the mixtures at 135 ± 5 °C for 2 h; (iii) remove the materials from the oven, cool it to room temperature and separate the lumps, sieving the loose materials with

the aid of metal balls of approximately 9.5 mm in diameter; (iv) note down the tare of the container (W_r) and weigh the material passing the 2.0 mm opening mesh, together with the container (W_a); (v) take it to the ignition oven for asphalt calcination; (vi) weigh the material after calcination (W_b). The FAM asphalt content (A_c) is determined by Equation 1.

$$A_c = \frac{W_a - W_b}{W_a - W_r} * 100\% \tag{1}$$

The crystallization water present in the mineral aggregate was not considered in the FAM design method developed by Sousa *et al.* (2013). At very high temperatures, such as the one practiced in the ignition oven, the crystallizing water evaporates. Grasson Filho (2019) determined the crystallization water following the procedure described by ASTM D 6307 (2016) using 200 g of mineral aggregate. The aggregate is kept in the ignition oven for the same time used to calcine the asphalt binder. The calibration factor is given by Equation 2. The asphalt content ($T_{c,corrected}$) present in the FAM is determined by Equation 3.

$$C_f = \frac{W_2 - W_3}{W_2 - W_1} \tag{2}$$

where C_f: calibration factor; W_1: mass of the container [g]; W_2: mass of dry aggregate + container [g]; W_3: mass of dry aggregate + container after ignition oven[g];

$$A_{c,corrected} = \frac{W_a - \{W_r + (W_b - W_r)*(1+C_f)\}}{W_a - W_r} * 100\% \tag{3}$$

The method developed by Kommidi and Kim (2019) was used to compact the FAMs. In the first stage of this method, the fine aggregates (200 g) and the asphalt binder are taken to the oven and heated at the mixing temperature (148 °C) for 30 minutes. Afterwards, about 150 g of loose mixture are prepared. The amount of material for each specimen (about 15 g) is separated into capsules and stored at 5 °C to avoid any kind of aging due to temperature variation. In the second stage, each capsule is taken to the oven together with the compaction mold for about 20 minutes until the mixture reaches the compaction temperature (137 ° C). Thereafter the material is statically compacted, producing specimens of 50 mm in hight and 12.7 mm in diameter. After compaction, 5 mm of the ends of the specimen are cut in an attempt to obtain a uniform air voids distribution along the specimen. In this method, all samples are produced with the same height and the air voids are controlled by means of the mass released into the mold (Equation 4).

$$M = \frac{Gmm*(1-Vv)\pi d^2 h}{4} \tag{4}$$

where M: FAM mass to be compacted [g]; Gmm: theoretical maximum density [g/cm^3]; Vv: estimated air voids content [%]; d: sample diameter [cm]; h: sample height [cm].

This compaction method allowed significant reduction in the amount of material used to prepare the specimens (around 79% less) when compared to the compaction in the SGC (specimen of 10 cm in diameter and 5 cm in hight). Moreover, this method allows a greater control of the air voids, which caused a significant reduction in the variability of the results obtained for the replicates.

The control FAM is referred to as FAM 01, and that one derived from the mixture with IOT is referred to as FAM 02. The following FAM binder contents were found after applying the method developed by Sousa *et al.* (2013) and adopting the calibration factor proposed by Grasson Filho (2019): 8.8% for FAM 01 and 8.7% for FAM 02.

2.5. Moisture-induced damage test

The moisture-induced damage test was carried according to ASTM D 4867-09 using the HMA mixture specimens. Six specimens were produced for each HMA mixture, three of them for the indirect tension test before moisture conditioning, and other three for the same test after moisture conditioning. All of the specimens were produced with a target air voids equal to 6.5 ± 0.5%.

The procedure adopted for conditioning the FAM specimens was the same used to condition the HMA mixture specimens. One of the most common methods to evaluate the FAM moisture susceptibility is to compare some material property, such as complex modulus or number of cycles to failure (N_f), before and after the moisture conditioning (Vasconcelos *et al.* 2006; Masad *et al.*, 2006; Caro *et al.*, 2012). Here, the moisture susceptibility was evaluated by comparing the $G*_{LVE}$ and the FAM fatigue factor (FFF) of the specimens tested in the DSR. It should be noted that FAMs with air voids of 4.0 ± 0.2% were used in the traditional fatigue analysis, and FAMs with 6.5 ± 0.2% air voids were used to assess the moisture-induced damage.

2.6. Damage tests

The damage tests of the FAM specimens were performed in the DSR. Two specimens of each FAM were tested to determine the linear viscoelasticity region ($G*_{LVE}$) by means of an oscillatory stress sweep test ranging from 5 to 450 kPa at 25 °C and 1 Hz. This procedure allows one to define the stress at which the fingerprint test will be performed, in order to obtain the viscoelastic linear properties ($G*_{LVE}$ and m), in such a way that no damage is imposed to the specimens. The complex modulus at the linear viscoelasticity limit ($G*_{LVE}$) has been defined as the one corresponding to 90% of the initial complex modulus ($G*$).

The fingerprint tests are conducted prior to the damage tests, and the same specimen is used in both tests. In the fingerprint, the $G*$ values are obtained at loading frequencies ranging from 30 to 0.5 Hz at 25 °C. Data obtained in the fingerprint is used in the calculation of the relaxation rate (m) of each specimen. The damage evolution rate (α) is equal to $1/m$. $G*_{LVE}$ is the average of the values obtained at 1 Hz. Three loading cycles were applied at each frequency, and a 5-minute interval was introduced for material recovery between frequencies.

The damage tests were performed at 1 Hz and 25 °C. The control specimens were tested at 250 kPa and the moisture-conditioned samples at 200 kPa. The G* values were registered every 30 seconds. Three specimens of each FAM were tested in order to obtain the curves of G* as a function of time. The shear stress, the strain and the complex modulus were transformed into their corresponding pseudo-variables. The pseudostiffness (C_k) for each loading cycle (k) was calculated by Equation 5, where G_k* is the complex modulus in each loading cycle, $|G*_{LVE}|$ is the complex modulus obtained in the fingerprint test at 1 Hz, and I is a factor that adjusts the initial pseudostiffness to the unity.

$$C_k = \frac{G_k^*}{I\left|G_{LVE}^*\right|} \tag{5}$$

The accumulated damage (S) was calculated according to the corresponding number of cycles (N), according to Equation 6, where $S_{u,0}$ is the material internal state variable at the beginning of each cycle, $t_i - t_{i-1}$ is the interval between cycles, and ε^R is the pseudostrain. These calculations allow one to build the pseudostiffness (C) vs accumulated damage (S) curves.

$$S \equiv S_{u,0} + \sum_{k=1}^{N} \left[\frac{I}{2}(\varepsilon^R)^2(C_{i-1}-C_i) \right]^{\alpha/(1+\alpha)} (t_i - t_{i-1})^{1/(1+\alpha)} \qquad (6)$$

Based on the average linear viscoelastic properties of three specimens of each FAM, three individual C vs S curves were built. An average C vs S curve was adjusted by taking the three individual curves as reference. These curves provide information to build the fatigue curves, by following the model developed by Kim and Little (2005). Equation 7 presents the fatigue model, which allows the estimation of the number of loading cycles (N_f) required to degrade the material to a certain level of damage (S_f). The failure criterion used was a 50% reduction of the initial pseudostiffness.

$$N_f \equiv A(\varepsilon^R)^{-B} \qquad (7)$$

The model coefficient A was obtained by means of Equation 8, where f is the test frequency. The coefficients C_1 and C_2 were obtained by adjusting a power law (Equation 9) to the average C vs S curve of each material. The coefficient B was calculated according to Equation 10.

$$A = f\left\{\frac{1}{2}C_1C_2\right\}^{\alpha} \left\{1+\alpha(1-C_2)\right\}^{-1} S_f^{1+[1+\alpha(1-C_2)]} \qquad (8)$$

$$C = 1 - C_1(S)^{C_2} \qquad (9)$$

$$B = 2\alpha \qquad (10)$$

The FAMs were ranked using the criteria proposed by Nascimento *et al.* (2014), which defined the mixture fatigue factor (MFF) as the area below the fatigue curve in the log-log space, between the 0.01% and 0.02% strains. In this analysis, it was assumed that the strains suffered by the asphalt mixture occur entirely at the FAM scale.

3. RESULTS, ANALYSIS AND DISCUSSION
3.1. Linear viscoelastic properties

Table 3 presents the linear viscoelastic properties of the FAMs obtained by means of the fingerprint tests.

Table 3 – Viscoelastic properties of the FAMs

Material	Specimen	Air voids (%)	G^*_{LVE} (Pa)	G^*_{LVE} average (Pa)	δ	γ (µstrain)	α	α average
FAM 01	1	4.0	6.26E+08		40	24	2.398	
	2	3.9	6.59E+08	6.40E+08	41	23	2.257	2.329
	3	4.0	6.34E+08		40	24	2.334	
FAM 02	1	4.1	4.65E+08		47	32	1.933	
	2	4.0	4.36E+08	4.65E+08	46	30	2.010	2.015
	3	4.0	4.95E+08		48	35	2.103	
FAM 01 (control)	1	6.3	4.14E+08		45	36	2.032	
	2	6.6	4.50E+08	4.44E+08	44	33	2.063	2.053
	3	6.6	4.66E+08		45	32	2.065	
FAM 01 (conditioned)	4	6.6	1.91E+08		47	79	1.778	
	5	6.6	1.84E+08	1.86E+08	46	82	1.834	1.810
	6	6.4	1.82E+08		48	83	1.817	
FAM 02 (control)	1	6.3	3.78E+08		46	37	1.950	
	2	6.5	3.33E+08	3.58E+08	48	34	1.880	1.916
	3	6.5	3.63E+08		46	32	1.917	
FAM 02 (conditioned)	4	6.4	2.91E+08		49	52	1.766	
	5	6.6	3.26E+08	2.97E+08	46	48	1.843	1.782
	6	6.6	2.75E+08		51	54	1.739	

The addition of IOT led to the reduction of the $G*_{LVE}$ values and increase of the phase angle (δ) of the specimens. In addition to this, IOT provided greater strains (γ) at the end of the fingerprint test, and lower damage evolution rates (α). These findings suggest that the mixtures prepared with IOT became less stiff. In general, the moisture-conditioned FAMs showed a considerable reduction in complex modulus, a slight increase in phase angle, and significantly higher strains as compared to the control FAMs. However, after moisture-conditioning, the FAM produced with IOT (FAM 02) showed greater values of $G*_{LVE}$ than those of FAM 01, and lower damage evolution rates. These results indicate that the mixtures prepared with IOT present lower moisture susceptibility, showing that the replacement is technically advantageous.

3.2. Moisture-induced damage

Table 4 shows the average tensile strength (TS) values of the HMA mixtures and the tensile strength ratio (RRT), which is the ratio between the average TS values of the moisture-conditioned specimens and the average TS values of the dry specimens. Table 4 also shows the comparison between the average $G*_{LVE}$ values of the FAMs and the ratio between the $G*_{LVE}$ values.

Table 4– Effects of moisture-induced damage on TS and $G*_{LVE}$

Material	Property	Dry samples	Moisture-conditioned samples	Ratio (%)
HMA 01	TS (MPa)	1.274	0.850	66.7
HMA 02	TS (MPa)	1.327	0.924	69.6
FAM 01	$G*_{LVE}$ (Pa)	4.44E+08	1.86E+08	41.9
FAM 02	$G*_{LVE}$ (Pa)	3.58E+08	2.97E+08	83.0

The results showed that the addition of IOT caused a slight increase in the tensile strength. Regarding moisture susceptibility, the IOT significantly improved the behavior at both scales, since the TSR value increased from 66.7% (HMA 01) to 69.6% (HMA 02), and the ratio between the $G*_{LVE}$ values of the FAMs increased from 41.9% (FAM 01) to 83.0% (FAM 02).

This improvement can be explained by the presence of iron oxide (Fe_2O_3). Recent papers have shown that the presence of this mineral enhances adhesiveness of the asphalt binder to the stone matrix in asphalt mixtures (Moura *et al.*, 2019; Cala *et al.* 2019). The IOT from flotation process has approximately 4% Fe2O3, which is supposed to have some beneficial effects on moisture susceptibility.

3.3. Characteristics curves C *vs* S and fatigue models

Due to the variability of $G*_{LVE}$ and α values among replicates, a replicate can generate a *C vs S* curve slightly different from the other ones. In order to manage the effects of variability among replicates, the following method was used to build the *C vs S* curve of each material: (i) test three specimens of each FAM, (ii) build the *C vs S* curves with the mean linear viscoelastic properties, and (iii) adjust an average curve which is representative of the three specimens. The coefficient A of the fatigue model of each FAM was calculated with basis on the coefficients C_1 and C_2, which were derived from fitting a power law to the average *C vs S* curve.
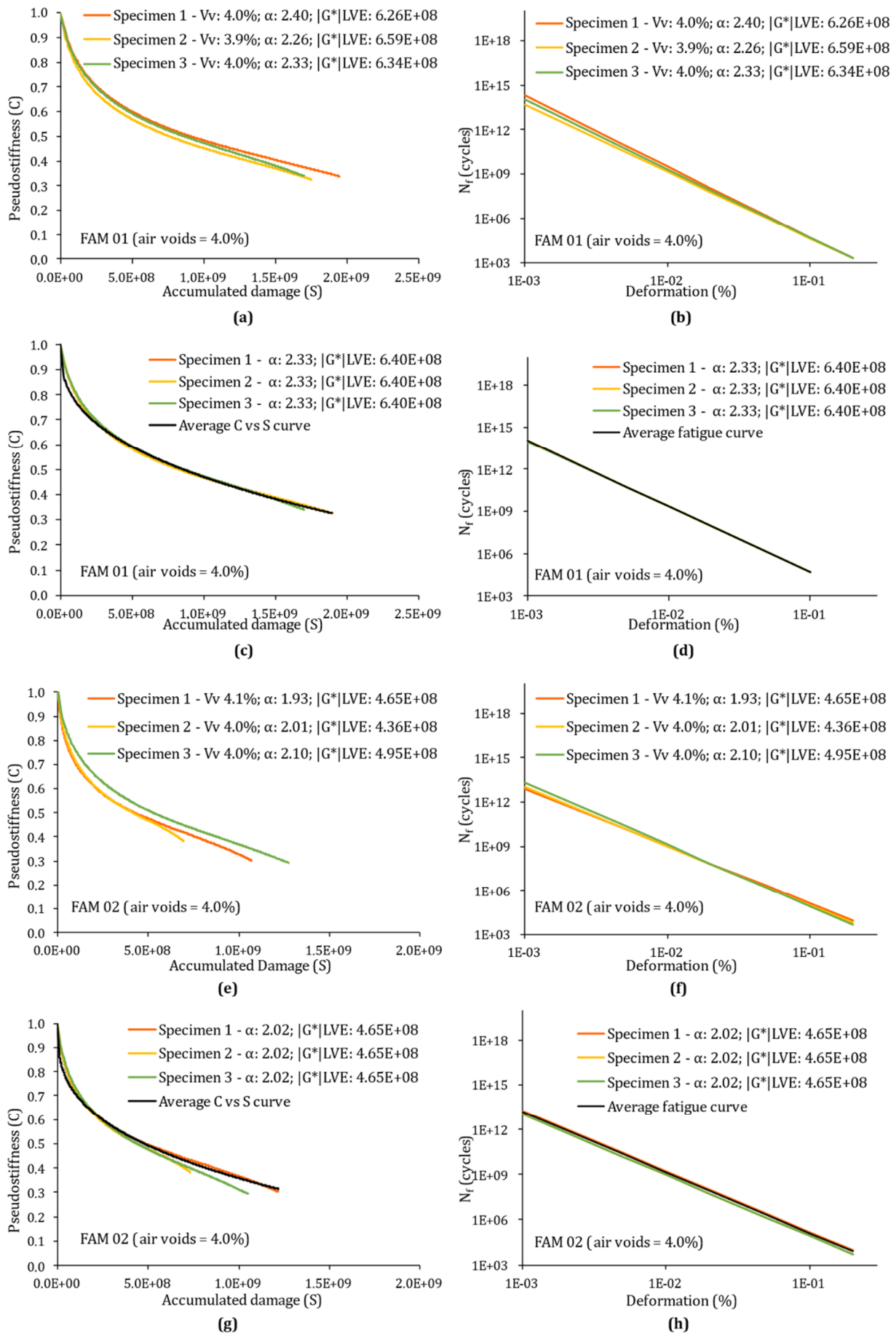
Figure 3. *C vs S* curves and fatigue curves for FAM 1 [(a) to (d)] and FAM 2 [(e) to (h)] (air voids = 4.0%)
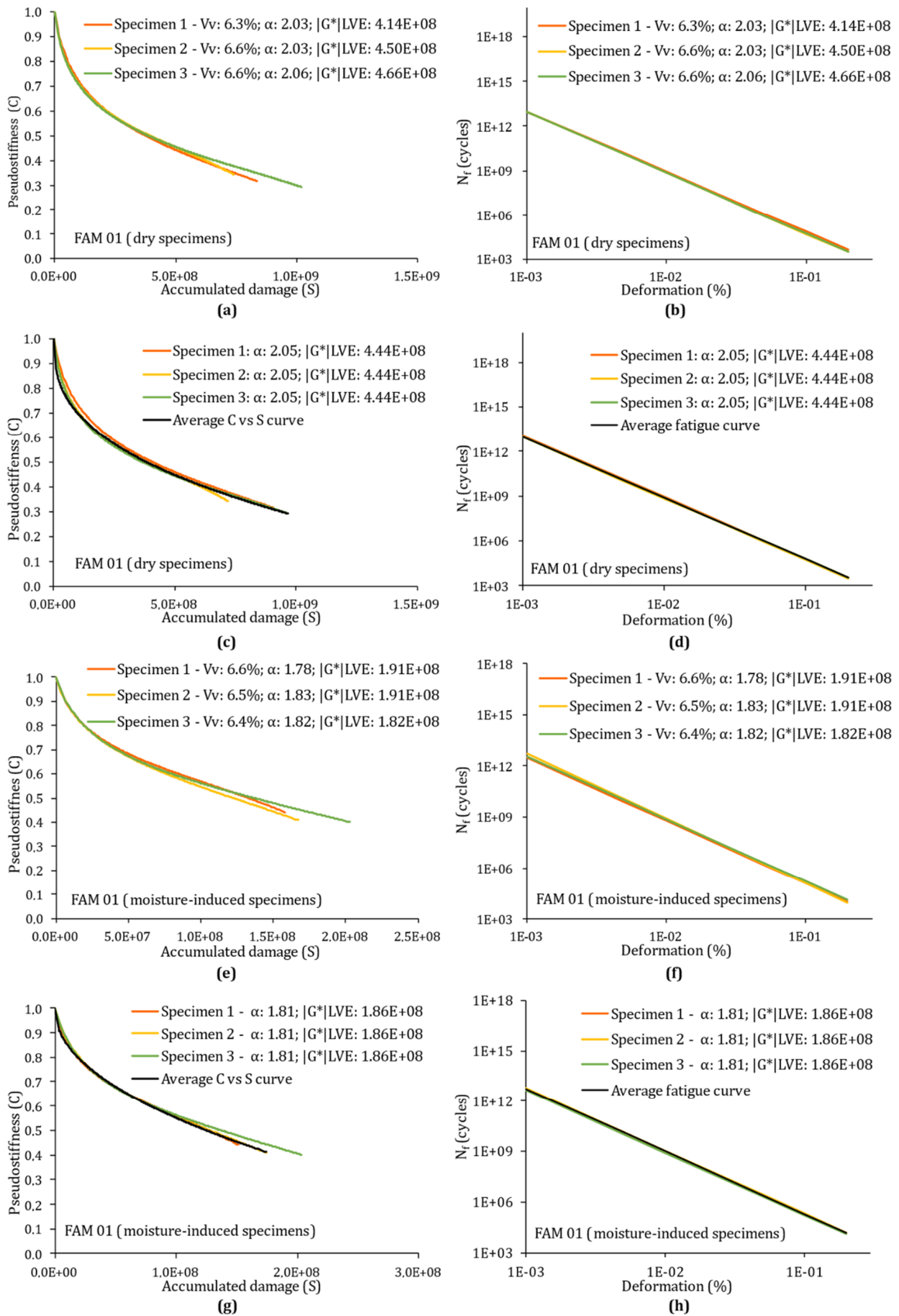
Figure 4. *C vs S* and fatigue curves of FAM 1 (dry specimens) [a-d] and (moisture-induced specimens) [e-h]
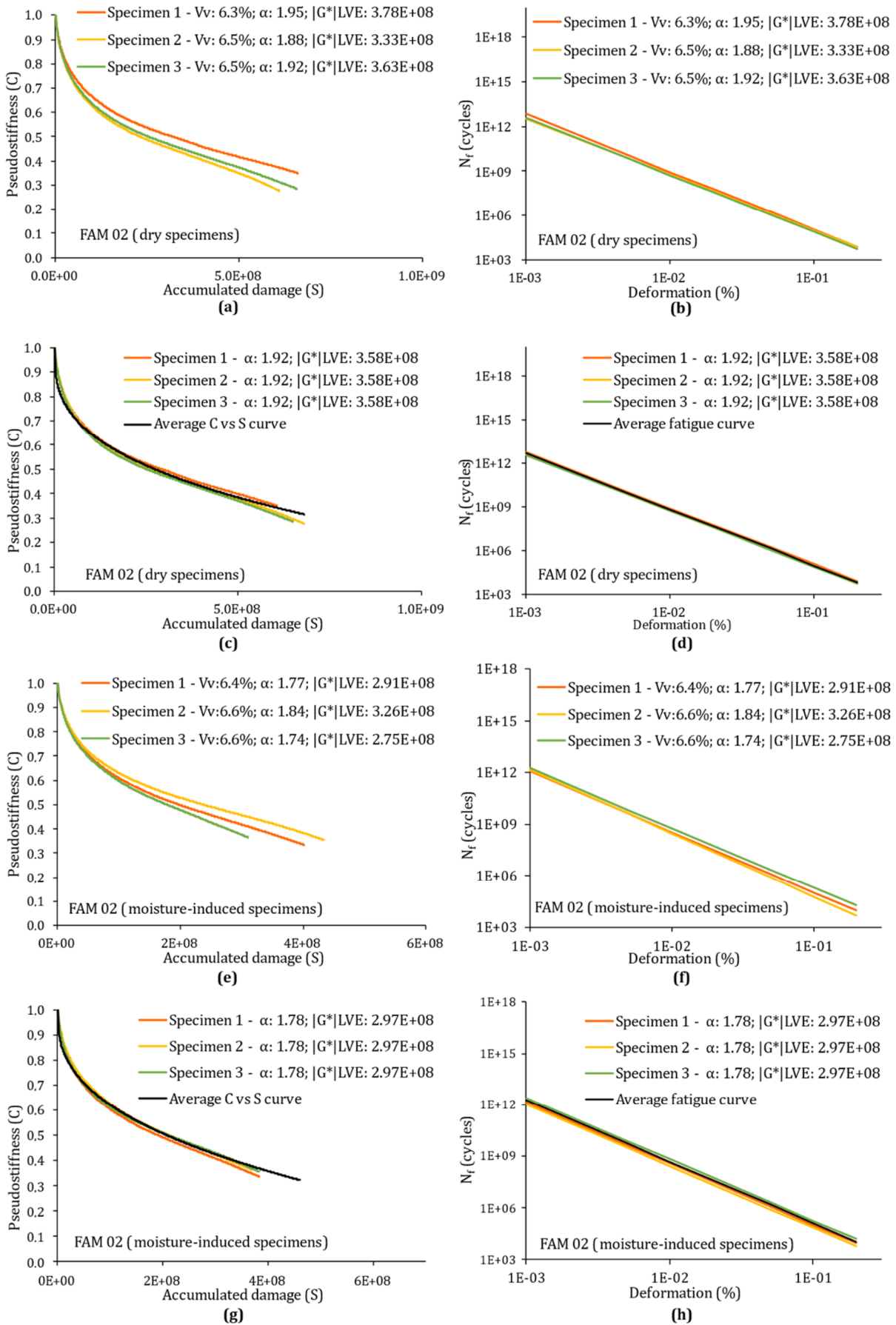
Figure 5. *C vs S* and fatigue curves of FAM 2 (dry specimens) [a-d] and (moisture-induced specimens) [e-h]
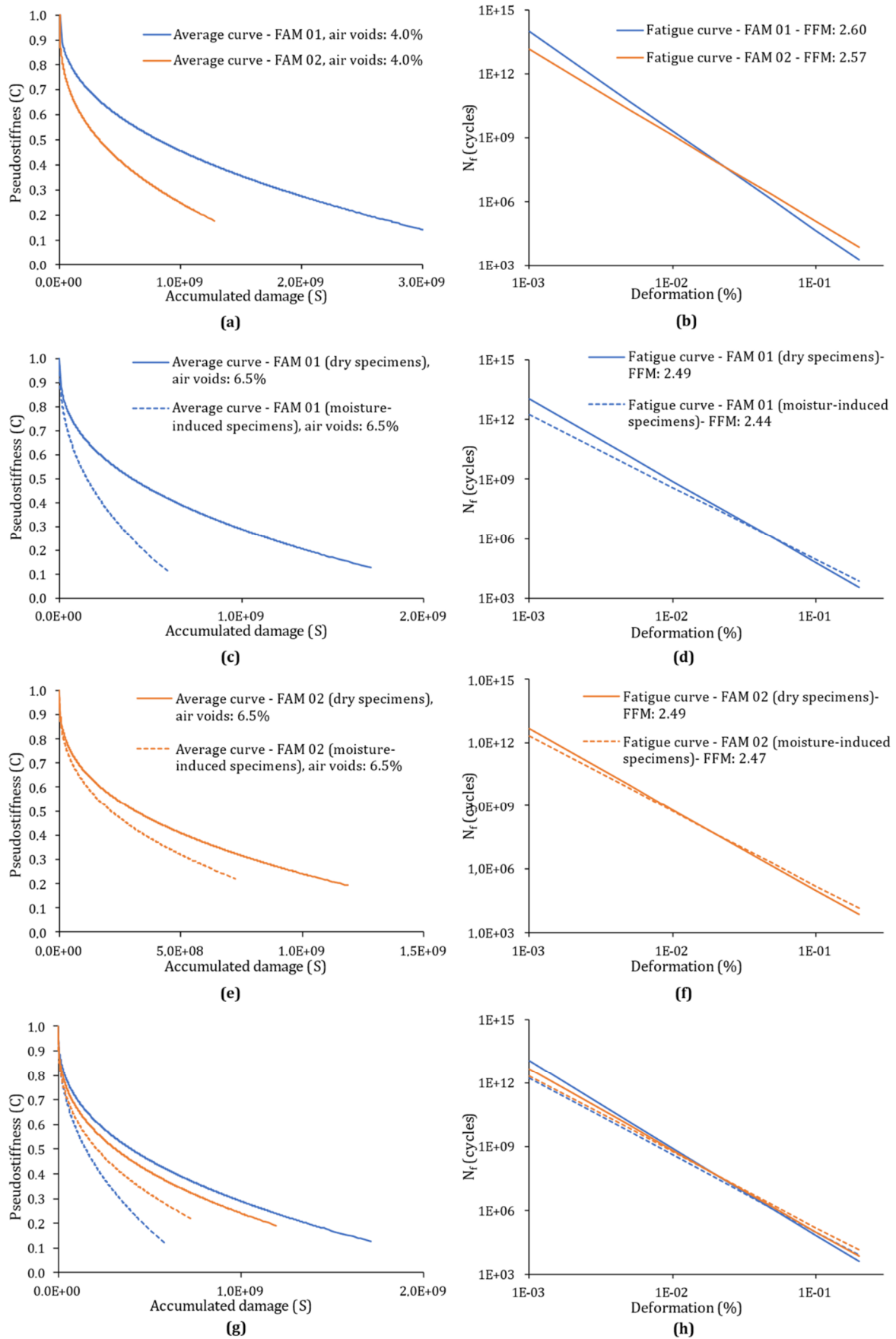
Figure 6. Comparison of average *C vs S* curves and associated fatigue models

Figure 3 shows the C vs S curves and the fatigue curves of FAMs 01 and 02 with 4.0% air voids, where Figure 3(a) depicts the individual C vs S curves, Figure 3(b) shows the fatigue curves generated with basis on the individual C vs S curves, Figure 3(c) presents (i) the C vs S curves built by using the average linear viscoelastic properties and (ii) the average C vs S curve, Figure 3(d) brings (i) the fatigue curves generated with basis on the C vs S curves built by using the average linear viscoelastic properties and (ii) the average fatigue curve built with basis on the average C vs S curve. Items from (a) to (d) refer to FAM 01, and items from (e) to (h) in this same figure bring information for FAM 02.

Figures 4 and 5 show the C vs S curves and the fatigue curves of the moisture-conditioned specimens and the dry specimens of FAMs 01 and 02, respectively, both with 6.5% air voids. In these Figures, item (a) presents the individual C vs S curves, item (b) brings the fatigue curves derived from the individual C vs S curves, item (c) depicts (i) the C vs S curves built by using the average linear viscoelastic properties and (ii) the average C vs S curve, Figure (d) shows (i) the fatigue curves generated with basis on the C vs S curves built by using the average linear visco-elastic properties and (ii) the average fatigue curve built with basis on the average C vs S curve. Items (a) to (d) refer to the dry FAM specimens, and items from (e) to (h) bring the same information for the moisture-conditioned FAM specimens.

Figure 6 shows a comparison of all average C vs S curves and their associated fatigue curves: (a) C vs S curves of FAMs 01 and 02 with 4.0% air voids; (b) fatigue curves associated to the C vs S curves of FAMs 01 and 02 with 4.0% air voids; (c) C vs S curves of FAM 01 for dry and moisture-conditioned specimens (air voids = 6.5%); (d) fatigue curves associated to the C vs S curves of FAM 01 for dry and moisture-conditioned specimens (air voids = 6.5%); (e) C vs S curves of FAM 02 for dry and moisture-conditioned specimens (air voids = 6.5%); (f) fatigue curves associated to the C vs S curves of FAM 02 for dry and moisture-conditioned specimens (air voids = 6.5%); (g) comparison of the C vs S curves of dry and moisture-conditioned specimens of FAMs 01 and 02 (air voids = 6.5%); and (h) comparison of the fatigue curves associated to the C vs S curves for dry and moisture-conditioned specimens of FAMs 01 and 02 (air voids = 6.5%).

3.4. FAM fatigue factors

The FAMs were compared by means of the mixture fatigue factor (MFF). The MFF values presented in Figure 6 indicate that the addition of IOT increased the fatigue factor of the moisture-conditioned specimens (MFF equal to 2.47 for FAM 02 moisture-conditioned specimens and 2.44 for FAM 01 moisture conditioned specimens). It suggests the same as already observed when comparing the $G*_{LVE}$ values, i.e., the addition of IOT reduces the susceptibility of the FAMs to moisture. It is worth mentioning that the control FAMs not subjected to moisture-conditioning showed slightly higher MFF values as compared to those prepared with IOT. However, it cannot be assumed that the IOT will significantly affect fatigue performance, as the differences between the MFF values are small.

4. CONCLUSIONS

The HMA mixture produced with IOT presented an asphalt binder content higher than the one produced with conventional gneiss aggregates (5.4% versus 5.6%). On the other hand, the binder content of the FAM produced with IOT decreased (8.8% versus 8.7%).

The method proposed by Sousa *et al.* (2013) is experimental, and for this reason part of the fine aggregate and filler may be retained during sieving, which may explain the difference in the FAM binder contents.

The addition of IOT increased the tensile strength and improved the resistance to moisture-induced damage of the HMA mixtures. The presence of iron oxide in IOT contributed significantly to improve the adhesiveness of the asphalt mastic to the aggregates, providing greater resistance to moisture-induced damage. This finding was also corroborated by the results at the FAM scale, when the $G*_{LVE}$ values are compared.

As observed for the $G*_{LVE}$ and tensile strength values, the addition of IOT led to fatigue factors for FAM 02 which are higher than those observed for FAM 01, showing that the incorporation of IOT resulted in FAMs with lower moisture susceptibility. The fatigue factors of the specimens of FAM 02 produced with IOT at the dry condition was equivalent to FAM 01 (no IOT). Nevertheless, the FAM with 4.0% air voids and without IOT showed MFF values slightly higher than the MFF values of the FAM with IOT.

In spite of what was observed for the FAM specimens without moisture-conditioning and 4.0% air voids, the difference between the MFF values resulted very small (difference at the second decimal place) and the fatigue curves overlapped, indicating similar fatigue behavior. The overall results obtained in this study showed that iron ore tailings may be technically feasible as raw material for the production of asphalt mixtures.

REFERENCES

AASHTO T 209 (2012) M*ethod of test for theoretical maximum specific gravity (Gmm) and density of hot mix asphalt (HMA)*. American Association of State Highway and Transportation Officials.

Agência Nacional de Mineração - ANM. (2020) Anuário Mineral Brasileiro*: Principais Substâncias Metálicas*. v. 1, 37 p.

Apaza, F. R.; A. C. R. Guimarães; M. A. S. Sousa e C. D. Castro (2018) Estudo sobre a utilização de Resíduo de Minério de Ferro em microrrevestimento asfáltico. *Transportes,* v. 26, n. 2, p. 118–138. DOI:10.14295/transportes.v26i2.1254.

Arambula, E.; E. Masad e A. Martin (2007) Moisture Susceptibility of Asphalt Mixtures with Known Field Performance: Evaluated with Dynamic Analysis and Crack Growth Model. *Transportation Research Record: Journal of the Transportation Research Board,* v. 2001, p. 20–28. DOI:10.3141/2001-03

ASTM D4867 (2009) *Standard test method for effect of moisture on asphalt concrete paving mixtures*. American Society for Testing and Materials.

ASTM D6926 (2013) *Standard practice for preparation of asphalt mixture specimens using Marshall apparatus*. American Society for Testing and Materials.

ASTM D6307 (2019) *Standard test method for asphalt content of asphalt mixture by ignition method*. American Society for Testing and Materials.

ASTM D6373 (2016) *Standard specification for performance graded asphalt binder*. American Society for Testing and Materials.

Bastos, L. A. de C. *et al.* (2016) Using iron ore tailings from tailing dams as road material. *Construction and Building Materials,* v. 112, n. 10, p. 988–995. DOI: 10.1061/(ASCE)MT.1943-5533.0001613.

Bhasin, A. (2006) *Development of Methods to Quantify Bitumen-Aggregate Adhesion and Loss of Adhesion Due to Water*. 2006. 146 p. Dissertation (PhD) Texas A&M Unversity. Austin. 2006. Disponível em: <https://core.ac.uk/download/pdf/4272833.pdf> (acesso em 17/08/2021).

Campanha, Â. (2011) *Caracterização dos rejeitos de minério de ferro para uso em pavimentação*. 2011. 90 p. Thesis (MSc) - Universidade Federal de Viçosa, Viçosa.. Disponível em: <https://www.locus.ufv.br/handle/123456789/3752> (acesso em 07/09/2021).

Campos, B. K. C. e F. B. Santos (2017) *Análise do Comportamento Mecânico de Misturas Asfálticas Com Adição do Rejeito de Flotação de Minério de Ferro*. 2017. 215 p. Trabalho Final de Graduação (Engenharia da Mobilidade) - Universidade Federal de Itajubá, Campus Itabira, Itabira.

Cala, A.; S. Caro; M. Lleras e Y. Rojas-Agramonte (2019) Impact of the chemical composition of aggregates on the adhesion quality and durability of asphalt-aggregate systems. *Construction and Building Materials,* v. 216, p. 661–672. DOI: 10.1016/j.conbuildmat.2019.05.030.

Caro, S. *et al.* (2008a) Probabilistic Analysis of Fracture in Asphalt Mixtures Caused by Moisture Damage*. Transportation Research Record: Journal of the Transportation Research Board*, v. 2057, n. Table 1, p. 28–36. DOI: 10.3141/2057-04.

Caro, S. *et al.* (2008b) Moisture susceptibility of asphalt mixtures, Part 1: Mechanisms. *International Journal of Pavement Engineering*, v. 9, n. 2, p. 81–98. DOI: 10.1080/10298430701792128.

Caro, S. *et al.* (2012) Analysis of moisture damage susceptibility of warm mix asphalt (WMA) mixtures based on Dynamic Mechanical Analyzer (DMA) testing and a fracture mechanics model. *Construction and Building Materials,* v. 35, p. 460–467. DOI: 10.1016/j.conbuildmat.2012.04.035

Castelo Branco, V. *et al.* (2008) Fatigue Analysis of Asphalt Mixtures Independent of Mode of Loading. *Transportation Research Record: Journal of the Transportation Research Board*, v. 2057, p. 149–156. DOI: 10.3141/2057-18.

Coutinho, R.P. *et al.* (2010) *Multiscale approach for characterization of asphaltic materials designed in Brazil and Spain.* 11th International Conference on Asphalt Pavements – ISAP, Japan.

Coutinho, R. P. (2012) *Utilização da parte fina de misturas asfálticas para avaliação do dano por fadiga.* 2012. 96 p. Thesis (MSc) – Departamento de Engenharia de Transportes, Universidade Federal do Ceará, Fortaleza. Disponível em: <http://www.repositorio.ufc.br/handle/riufc/4888> (acesso em 17/08/2021).

DNIT 031 - ES (2006) *Pavimentação Asfáltica – Concreto Asfáltico – Especificação de Serviço*. Departamento Nacional de Infraestrutura de Transportes, Rio de Janeiro.

DNIT 095 - EM (2006) *Cimentos asfálticos de petróleo – Especificação de material*. Departamento Nacional de Infraestrutura de Transportes, Rio de Janeiro.

Fernandes, G. (2005) *Comportamento de Estruturas de Pavimentos Ferroviários com a Utilização de Solos Finos e/ou Resíduo de Mineração de Ferro Associados a Geossintéticos*. 2005. 253 p. Dissertation (PhD) - Departamento de Engenharia Civil e Ambiental, Universidade de Brasília, Brasília.

Fonseca, J. F. *et al.* (2019) Evaluation of Effects of Filler By-Products on Fine Aggregate Matrix Viscoelasticity and Fatigue-Fracture Characteristics*. Journal of Materials in Civil Engineering*, v. 31, n. 10, p. 04019240. DOI: 10.1061/(ASCE)MT.1943-5533.0002891.

Freire, R. A. *et al.* (2017) Aggregate Maximum Nominal Sizes' Influence on Fatigue Damage Performance Using Different Scales. *Journal of Materials in Civil Engineering*, v. 29, n. 8, p. 04017067. DOI: 10.1061/(ASCE)MT.1943-5533.0001912

Galhardo, D. C. (2015) *Estudo sobre a viabilidade técnica da utilização de rejeitos de mineração de ferro em camadas de pavimentos rodoviários.* 2015. 186 p. Thesis (MSc) - Instituto Militar de Engenharia, Rio de Janeiro, Disponível em: <https://bdex.eb.mil.br/jspui/handle/123456789/7882> (acesso em 07/09/2021).

Grasson Filho, A. (2019) *Evaluation of the specific surface method as a tool to determine the asphalt content of fine aggregate matrices (FAM)*. 2017. 75 p. Thesis (MSc) - Escola de Engenharia de São Carlos, Universidade de São Paulo, São Carlos. Disponível em: <https://www.Dissertations.usp.br/Dissertations/disponiveis/18/18143/tde-16122019-141054/pt-br.php> (acesso em 17/08/2021).

Gudipudi, P. e B. S. Underwood (2015) Testing and Modeling of Fine Aggregate Matrix and Its Relationship to Asphalt Concrete Mix*. Transportation Research Record: Journal of the Transportation Research Board*, v. 2507, p. 120–127. DOI: 10.3141/2507-13.

Gudipudi, P. e B. S. Underwood (2017) Use of Fine Aggregate Matrix Experimental Data in Improving Reliability of Fatigue Life Prediction of Asphalt Concrete. *Transportation Research Record: Journal of the Transportation Research Board*, v. 2631, p. 65–73. DOI: 10.3141/2631-07.

Karki, P.; R. Li e A. Bhasin (2015) Quantifying overall damage and healing behaviour of asphalt materials using continuum damage approach*. International Journal of Pavement Engineering*, v. 16, n. 4, p. 350–362. Disponível em: <https://www.tandfonline.com/doi/abs/10.1080/10298436.2014.942993> (acesso em 17/08/2021). DOI: 10.1080/10298436.2014.942993.

Kim, Y. e D. N. Little (2005) *Development of Specification-Type Tests to Assess the Impact of Fine Aggregate and Mineral Filler on Fatigue Damage*. Federal Highway Administration, U.S. Department of Transportation and Texas Transportation Institute, 116 p.

Kim, Y.; D. Little e I. Song (2003) Effect of Mineral Fillers on Fatigue Resistance and Fundamental Material Characteristics: Mechanistic Evaluation. *Transportation Research Record: Journal of the Transportation Research Board*, v. 1832, n. 03, p. 1–8, 2003. DOI:10.3141/1832-01.

Klug, A. B. (2017) *Evaluation of the fatigue performance of fine aggregate matrices prepared with reclaimed asphalt pavements and shale oil residue.* 2017. 162 p. Thesis (Master in Science) - Departamento de Engenharia de Transportes, Escola de Engenharia de São Carlos, Universidade de São Paulo, São Carlos, SP. Disponível em: <https://www.Dissertations.usp.br/Dissertations/disponiveis/18/18143/tde-19022018-112755/en.php> (acesso em 17/08/2021).

Kommidi, S. R. e Y.R. Kim (2019) Fatigue characterization of binder under the influence of aging in two length scales: sand asphalt mortar and parallel plate binder film*. In: *Transportation Research Board*. Washington, DC. DOI: 10.1016/j.conbuildmat.2019.117588.

Kumar B. N. S.; R. Sushas; S. U. Shet e J. M. Srishaila (2014) Utilization of iron ore tailings as replacement to fine aggregates in cement concrete pavements. *International Journal of Research in Engineering and Technology*, v. 03. DOI: 10.15623/ijret.2014.0307063.

Masad, E. *et al.* (2006) Characterization of hma moisture damage using surface energy and fracture properties. Asphalt Paving Technology: *Association of Asphalt Paving Technologists-Proceedings of the Technical Sessions,* v. 75. Disponível em: < https://trid.trb.org/view/798239> (acesso em 7/08/2021).

Moura, B. L. Riz de.*et al.* (2019) Avaliação da adesividade ligante-escória de alto-forno resfriada ao ar (ACBFS) e de aciaria (LD) usando técnicas de análise de superficies. In: *33° Congresso de Pesquisa e Ensino em Transportes da ANPET*. Anais… Balneário Camboriú, 2019. p. 1799-1811. Disponível em: <https://anpet.org.br/anais/documentos/2019/Infraestrutura/Materiais%20e%20Tecnologias%20Ambientais%20I/2_275_AC.pdf> (acesso em 17/08/2021).

Nascimento L. A. H. *et al.* (2014) Uso da mecânica do dano contínuo na caracterização de misturas asfálticas brasileiras. In: *21º Encontro de Asfalto*, 2014, IBP, Rio de Janeiro.

Ng, A. K. Y. (2017) *Avaliação do comportamento ao dano por fadiga de matrizes de agregado fino preparadas com ligantes asfálticos modificados*. 2017. 201 p. Dissertation (PhD) - Escola de Engenharia de São Carlos, Universidade de São Paulo, São Carlos. Disponível em: < https://Dissertations.usp.br/Dissertations/disponiveis/18/18143/tde-03012018-122026/pt-br.php> (acesso em 17/08/2021).

Oliveira, I. C. S. de. (2017) *Estudo da adição do rejeito de flotação de minério de ferro em dosagem de misturas asfálticas.* 2017. 73 p. Trabalho Final de Graduação (Engenharia da Mobilidade) - Universidade Federal de Itajubá, Campus Itabira, Itabira.

Palvadi, N. S. (2011) *Measurement of material properties related to self-healing based on continuum and micromechanics approach*. 2011. 87 p. Thesis (MSc) - Texas A&M University, Austin. Disponível em: < https://repositories.lib.utexas.edu/handle/2152/ETD-UT-2011-08-4274> (acesso em 17/08/2021).

Palvadi, S.; A. Bhasin e D. N. Little (2012) Method to quantify healing in asphalt composites by continuum damage approach. *Transportation Research Record: Journal of the Transportation Research Board*, v. 2296, n. 1, p. 86–96. Disponível em: <https://journals.sagepub.com/doi/abs/10.3141/2296-09> (acesso em 17/08/2021). DOI: 10.3141/2296-0.

Prowell, B. D.; J. Zhang e E. R. Brown (2005) *Aggregate Properties and the Performance of Superpave Designed Hot Mix Asphalt*. Report NCHRP-539, National Cooperative Highway Research Program. National Research Council. Washington, D.C.

Rodrigues, J. A. *et al.* (2019) Crack modeling of bituminous materials using extrinsic nonlinear viscoelastic cohesive zone (NVCZ) model. *Construction and Building Materials*, v. 204, p. 520-529. DOI: 10.1016/j.conbuildmat.2019.01.215.

Sant'ana Filho, J. N. *et al.* (2017) Technical and environmental feasibility of interlocking concrete pavers with iron ore from tailings dams. *Journal of Materials in Civil Engineering*, v. 29, n. 9. DOI: 10.1061/(ASCE)MT.1943-5533.0001937

Silva, F. L.; F. G. S. Araújo; C. G. Castro e F. L. V. Kruger (2015) Results of the leaching, water absorption and mold release for concrete blocks with the addition of the concentration tailings of iron ore. *Materials Science Forum (Online),* v. 820, p. 549-552. DOI: 10.4028/www.scientific.net/MSF.820.549.

Silva, R. G. O e G. Fernandes (2013) Estudo laboratorial do desempenho mecânico de misturas asfálticas com escória de aciaria e resíduos industriais de minério de ferro. *Revista Pavimentação*, v. VIII, p. 44-52.

Sousa, P. *et al.* (2013) New design method of fine aggregates mixtures and automated method for analysis of dynamic mechanical characterization data. *Construction and Building Materials*, v. 41, p. 216–223. DOI: 10.1016/j.conbuildmat.2012.11.038.

Souza, T., D. de; B. de A. e Silva; A. C. R. Guimarães e A. R. Mesquita (2020) Propriedades mecânicas de concretos asfálticos dosados com rejeitos do beneficiamento magnético a seco do minério de ferro. *Transportes*, v. 28, n. 1, p. 175-186. DOI:10.14295/transportes.v28i1.1964.

Underwood, B. S. e Y. R. Kim (2013) Nonlinear Viscoelastic Behavior of Asphalt Concrete and Its Implication for Fatigue Modeling. *Transportation Research Record: Journal of the Transportation Research Board*, v. 2373, n. 1, p. 100–108. DOI: 10.3141/2373-11.

Vasconcelos, K. L. *et al.* (2006) Avaliação do Dano por Umidade Induzida e da Recuperação de Trincas em Mástique. In: *XVIII Encontro De Ligante Asfáltico Instituto*, 2006. Anais… Rio de Janeiro, 2017. p. 1-8.

Vasconcelos, K. L.; D. N. Little; A. Bhasin (2010) Influence of reduced production temperatures on the adhesive properties of aggregates and laboratory performance of fine aggregate-asphalt mixtures. *Road Materials and Pavement Design*, v. 11, n. 1, p. 47–64. DOI: 10.1080/14680629.2010.9690259.

Wang, Z. *et al.* (2016) Utilization of magnetite tailings as aggregates in asphalt mixtures. *Construction and Building Materials*, v. 114, p. 392-399. DOI: 10.1016/j.conbuildmat.2016.03.139.

Zollinger, C. J. (2005) *Application of surface energy measurements to evaluate moisture susceptibility of asphalt and aggregates*. 2005. 133 p. Thesis (MSc) - Texas A&M University, Austin. Disponível em: <https://oaktrust.library.tamu.edu/handle/1969.1/2320> (acesso em 17/08/2021).